Astroparticle Physics 34 (2010) 314–326

Contents lists available at ScienceDirect

Astroparticle Physics

journal homepage: www.elsevier.com/locate/astropart

Update on the correlation of the highest energy cosmic rays with nearby extragalactic matter

The Pierre Auger Collaboration, P. Abreu [bj], M. Aglietta [aw], E.J. Ahn [by], D. Allard [z], I. Allekotte [a], J. Allen [cb], J. Alvarez Castillo [bc], J. Alvarez-Muñiz [bq], M. Ambrosio [aq], A. Aminaei [bd], L. Anchordoqui [cl], S. Andringa [bj], T. Antičić [u], A. Anzalone [av], C. Aramo [aq], E. Arganda [bn], K. Arisaka [cg], F. Arqueros [bn], H. Asorey [a], P. Assis [bj], J. Aublin [ab], M. Ave [af,ch], M. Avenier [ac], G. Avila [i], T. Bäcker [al], D. Badagnani [e], M. Balzer [ag], K.B. Barber [j], A.F. Barbosa [k], R. Bardenet [aa], S.L.C. Barroso [q], B. Baughman [cd], J.J. Beatty [cd], B.R. Becker [cj], K.H. Becker [ae], A. Bellétoile [ac], J.A. Bellido [j], C. Berat [ac], T. Bergmann [ag], X. Bertou [a], P.L. Biermann [ai], P. Billoir [ab], F. Blanco [bn], M. Blanco [bo], C. Bleve [ae,ap], H. Blümer [ah,af], M. Boháčová [ch,w], D. Boncioli [ar], C. Bonifazi [t,ab], R. Bonino [aw], N. Borodai [bh], J. Brack [bw], P. Brogueira [bj], W.C. Brown [bx], R. Bruijn [bs], P. Buchholz [al], A. Bueno [bp], R.E. Burton [bu], N.G. Busca [z], K.S. Caballero-Mora [ah], L. Caramete [ai], R. Caruso [as], A. Castellina [aw], O. Catalano [av], G. Cataldi [ap], L. Cazon [bj], R. Cester [at], J. Chauvin [ac], A. Chiavassa [aw], J.A. Chinellato [o], A. Chou [by,cb], J. Chudoba [w], R.W. Clay [j], E. Colombo [b], M.R. Coluccia [ap], R. Conceição [bj], F. Contreras [h], H. Cook [bs], M.J. Cooper [j], J. Coppens [bd,bf], A. Cordier [aa], U. Cotti [bb], S. Coutu [ce], C.E. Covault [bu], A. Creusot [bl], A. Criss [ce], J. Cronin [ch], A. Curutiu [ai], S. Dagoret-Campagne [aa], R. Dallier [ad], S. Dasso [f,d], K. Daumiller [af], B.R. Dawson [j], R.M. de Almeida [o,t], M. De Domenico [as], C. De Donato [bc,ao], S.J. de Jong [bd], G. De La Vega [g], W.J.M. de Mello Junior [o], J.R.T. de Mello Neto [t], I. De Mitri [ap], V. de Souza [m], K.D. de Vries [be], G. Decerprit [z], L. del Peral [bo], O. Deligny [y], A. Della Selva [aq], H. Dembinski [af], A. Denkiewicz [b], C. Di Giulio [ar], J.C. Diaz [ca], M.L. Díaz Castro [l], P.N. Diep [cm], C. Dobrigkeit [o], J.C. D'Olivo [bc], P.N. Dong [cm,y], A. Dorofeev [bw], J.C. dos Anjos [k], M.T. Dova [e], D. D'Urso [aq], I. Dutan [ai], J. Ebr [w], R. Engel [af], M. Erdmann [aj], C.O. Escobar [o], A. Etchegoyen [b], P. Facal San Luis [ch], H. Falcke [bd,bg], G. Farrar [cb], A.C. Fauth [o], N. Fazzini [by], A.P. Ferguson [bu], A. Ferrero [b], B. Fick [ca], A. Filevich [b], A. Filipčič [bk,bl], I. Fleck [al], S. Fliescher [aj], C.E. Fracchiolla [bw], E.D. Fraenkel [be], U. Fröhlich [al], B. Fuchs [k], W. Fulgione [aw], R.F. Gamarra [b], S. Gambetta [am], B. García [g], D. García Gámez [bp], D. Garcia-Pinto [bn], X. Garrido [af], A. Gascon [bp], G. Gelmini [cg], H. Gemmeke [ag], K. Gesterling [cj], P.L. Ghia [y,aw], U. Giaccari [ap], M. Giller [bi], H. Glass [by], M.S. Gold [cj], G. Golup [a], F. Gomez Albarracin [e], M. Gómez Berisso [a], P. Gonçalves [bj], D. Gonzalez [ah], J.G. Gonzalez [ah], B. Gookin [bw], D. Góra [ah,bh], A. Gorgi [aw], P. Gouffon [n], S.R. Gozzini [bs], E. Grashorn [cd], S. Grebe [bd], M. Grigat [aj], A.F. Grillo [ax], Y. Guardincerri [d], F. Guarino [aq], G.P. Guedes [p], J.D. Hague [cj], P. Hansen [e], D. Harari [a], S. Harmsma [be,bf], J.L. Harton [bw], A. Haungs [af], T. Hebbeker [aj], D. Heck [af], A.E. Herve [j], C. Hojvat [by], V.C. Holmes [j], P. Homola [bh], J.R. Hörandel [bd], A. Horneffer [bd], M. Hrabovský [x,w], T. Huege [af], A. Insolia [as], F. Ionita [ch], A. Italiano [as], S. Jiraskova [bd], K. Kadija [u], M. Kaducak [by], K.H. Kampert [ae], P. Karhan [v], T. Karova [w], P. Kasper [by], B. Kégl [aa], B. Keilhauer [af], A. Keivani [bz], J.L. Kelley [bd], E. Kemp [o], R.M. Kieckhafer [ca], H.O. Klages [af], M. Kleifges [ag], J. Kleinfeller [af], J. Knapp [bs], D.-H. Koang [ac], K. Kotera [ch], N. Krohm [ae], O. Krömer [ag], D. Kruppke-Hansen [ae], F. Kuehn [by], D. Kuempel [ae], J.K. Kulbartz [ak], N. Kunka [ag], G. La Rosa [av], C. Lachaud [z], P. Lautridou [ad], M.S.A.B. Leão [s], D. Lebrun [ac], P. Lebrun [by], M.A. Leigui de Oliveira [s], A. Lemiere [y], A. Letessier-Selvon [ab], I. Lhenry-Yvon [y], K. Link [ah], R. López [az], A. Lopez Agüera [bq], K. Louedec [aa], J. Lozano Bahilo [bp], A. Lucero [b,aw], M. Ludwig [ah], H. Lyberis [y], M.C. Maccarone [av], C. Macolino [ab,an], S. Maldera [aw], D. Mandat [w], P. Mantsch [by], A.G. Mariazzi [e], V. Marin [ad], I.C. Maris [ab], H.R. Marquez Falcon [bb], G. Marsella [au], D. Martello [ap], L. Martin [ad], O. Martínez Bravo [az], H.J. Mathes [af], J. Matthews [bz,cf], J.A.J. Matthews [cj], G. Matthiae [ar], D. Maurizio [at], P.O. Mazur [by], M. McEwen [bo], G. Medina-Tanco [bc], M. Melissas [ah], D. Melo [at], E. Menichetti [at], A. Menshikov [ag], C. Meurer [aj], S. Mičanović [u], M.I. Micheletti [b], W. Miller [cj], L. Miramonti [ao], S. Mollerach [a], M. Monasor [ch], D. Monnier Ragaigne [aa], F. Montanet [ac],

doi:10.1016/j.astropartphys.2010.08.010

B. Morales [bc], C. Morello [aw], E. Moreno [az], J.C. Moreno [e], C. Morris [cd], M. Mostafá [bw], S. Mueller [af], M.A. Muller [o], M. Münchmeyer [ab], R. Mussa [at], G. Navarra [aw,1], J.L. Navarro [bp], S. Navas [bp], P. Necesal [w], L. Nellen [bc], P.T. Nhung [cm], N. Nierstenhoefer [ae], D. Nitz [ca], D. Nosek [v], L. Nožka [w], M. Nyklicek [w], J. Oehlschläger [af], A. Olinto [ch], P. Oliva [ae], V.M. Olmos-Gilbaja [bq], M. Ortiz [bn], N. Pacheco [bo], D. Pakk Selmi-Dei [o], M. Palatka [w], J. Pallotta [c], N. Palmieri [ah], G. Parente [bq], E. Parizot [z], A. Parra [bq], J. Parrisius [ah], R.D. Parsons [bs], S. Pastor [bm], T. Paul [cc], V. Pavlidou [ch,2], K. Payet [ac], M. Pech [w], J. Pękala [bh], R. Pelayo [bq], I.M. Pepe [r], L. Perrone [au], R. Pesce [am], E. Petermann [ci], S. Petrera [an], P. Petrinca [ar], A. Petrolini [am], Y. Petrov [bw], J. Petrovic [bf], C. Pfendner [ck], N. Phan [cj], R. Piegaia [d], T. Pierog [af], M. Pimenta [bj], V. Pirronello [as], M. Platino [b], V.H. Ponce [a], M. Pontz [al], P. Privitera [ch], M. Prouza [w], E.J. Quel [c], J. Rautenberg [ae], O. Ravel [ad], D. Ravignani [b], B. Revenu [ad], J. Ridky [w], S. Riggi [as], M. Risse [al], P. Ristori [c], H. Rivera [ao], C. Rivière [ac], V. Rizi [an], C. Robledo [az], G. Rodriguez [bq], J. Rodriguez Martino [h,as], J. Rodriguez Rojo [h], I. Rodriguez-Cabo [bq], M.D. Rodríguez-Frías [bo], G. Ros [bo], J. Rosado [bn], T. Rossler [x], M. Roth [af], B. Rouillé-d'Orfeuil [ch], E. Roulet [a], A.C. Rovero [f], F. Salamida [af,an], H. Salazar [az], G. Salina [ar], F. Sánchez [b], M. Santander [h], C.E. Santo [bj], E. Santos [bj], E.M. Santos [t], F. Sarazin [bv], S. Sarkar [br], R. Sato [h], N. Scharf [aj], V. Scherini [ao], H. Schieler [af], P. Schiffer [aj], A. Schmidt [ag], F. Schmidt [ch], T. Schmidt [ah], O. Scholten [be], H. Schoorlemmer [bd], J. Schovancova [w], P. Schovánek [w], F. Schroeder [af], S. Schulte [aj], F. Schüssler [af], D. Schuster [bv], S.J. Sciutto [e], M. Scuderi [as], A. Segreto [av], M. Settimo [ap], A. Shadkam [bz], R.C. Shellard [k,l], I. Sidelnik [b], G. Sigl [ak], A. Śmiałkowski [bi], R. Šmída [af,w], G.R. Snow [ci], P. Sommers [ce], J. Sorokin [j], H. Spinka [bt,by], R. Squartini [h], J. Stapleton [cd], J. Stasielak [bh], M. Stephan [aj], E. Strazzeri [av], A. Stutz [ac], F. Suarez [b], T. Suomijärvi [y], A.D. Supanitsky [bc], T. Šuša [u], M.S. Sutherland [cd], J. Swain [cc], Z. Szadkowski [ae,bi], A. Tamashiro [f], A. Tapia [b], T. Tarutina [e], O. Taşcău [ae], R. Tcaciuc [al], D. Tcherniakhovski [ag], D. Tegolo [as,ay], N.T. Thao [cm], D. Thomas [bw], J. Tiffenberg [d], C. Timmermans [bf,bd], D.K. Tiwari [bb], W. Tkaczyk [bi], C.J. Todero Peixoto [s], B. Tomé [bj], A. Tonachini [at], P. Travnicek [w], D.B. Tridapalli [n], G. Tristram [z], E. Trovato [as], M. Tueros [e], R. Ulrich [ce,af], M. Unger [af], M. Urban [aa], J.F. Valdés Galicia [bc], I. Valiño [af], L. Valore [aq], A.M. van den Berg [be], B. Vargas Cárdenas [bc], J.R. Vázquez [bn], R.A. Vázquez [bq], D. Veberič [bl,bk], T. Venters [ch], V. Verzi [ar], M. Videla [g], L. Villaseñor [bb], H. Wahlberg [e], P. Wahrlich [j], O. Wainberg [b], D. Warner [bw], A.A. Watson [bs], K. Weidenhaupt [aj], A. Weindl [af], B.J. Whelan [j], G. Wieczorek [bi], L. Wiencke [bv], B. Wilczyńska [bh], H. Wilczyński [bh], M. Will [af], C. Williams [ch], T. Winchen [aj], L. Winders [cl], M.G. Winnick [j], M. Wommer [af], B. Wundheiler [b], T. Yamamoto [ch,3], P. Younk [bw], G. Yuan [bz], A. Yushkov [aq], B. Zamorano [bp], E. Zas [bq], D. Zavrtanik [bl,bk], M. Zavrtanik [bk,bl], I. Zaw [cb], A. Zepeda [ba], M. Ziolkowski [al]

[a] *Centro Atómico Bariloche and Instituto Balseiro (CNEA-UNCuyo-CONICET), San Carlos de Bariloche, Argentina*
[b] *Centro Atómico Constituyentes (Comisión Nacional de Energía Atómica/CONICET/UTN-FRBA), Buenos Aires, Argentina*
[c] *Centro de Investigaciones en Láseres y Aplicaciones, CITEFA and CONICET, Argentina*
[d] *Departamento de Física, FCEyN, Universidad de Buenos Aires y CONICET, Argentina*
[e] *IFLP, Universidad Nacional de La Plata and CONICET, La Plata, Argentina*
[f] *Instituto de Astronomía y Física del Espacio (CONICET-UBA), Buenos Aires, Argentina*
[g] *National Technological University, Faculty Mendoza (CONICET/CNEA), Mendoza, Argentina*
[h] *Pierre Auger Southern Observatory, Malargüe, Argentina*
[i] *Pierre Auger Southern Observatory and Comisión Nacional de Energía Atómica, Malargüe, Argentina*
[j] *University of Adelaide, Adelaide, SA, Australia*
[k] *Centro Brasileiro de Pesquisas Fisicas, Rio de Janeiro, RJ, Brazil*
[l] *Pontifícia Universidade Católica, Rio de Janeiro, RJ, Brazil*
[m] *Universidade de São Paulo, Instituto de Física, São Carlos, SP, Brazil*
[n] *Universidade de São Paulo, Instituto de Física, São Paulo, SP, Brazil*
[o] *Universidade Estadual de Campinas, IFGW, Campinas, SP, Brazil*
[p] *Universidade Estadual de Feira de Santana, Brazil*
[q] *Universidade Estadual do Sudoeste da Bahia, Vitoria da Conquista, BA, Brazil*
[r] *Universidade Federal da Bahia, Salvador, BA, Brazil*
[s] *Universidade Federal do ABC, Santo André, SP, Brazil*
[t] *Universidade Federal do Rio de Janeiro, Instituto de Física, Rio de Janeiro, RJ, Brazil*
[u] *Rudjer Bošković Institute, 10000 Zagreb, Croatia*
[v] *Charles University, Faculty of Mathematics and Physics, Institute of Particle and Nuclear Physics, Prague, Czech Republic*
[w] *Institute of Physics of the Academy of Sciences of the Czech Republic, Prague, Czech Republic*
[x] *Palacký University, Olomouc, Czech Republic*
[y] *Institut de Physique Nucléaire d'Orsay (IPNO), Université Paris 11, CNRS-IN2P3, Orsay, France*
[z] *Laboratoire AstroParticule et Cosmologie (APC), Université Paris 7, CNRS-IN2P3, Paris, France*
[aa] *Laboratoire de l'Accélérateur Linéaire (LAL), Université Paris 11, CNRS-IN2P3, Orsay, France*
[ab] *Laboratoire de Physique Nucléaire et de Hautes Energies (LPNHE), Universités Paris 6 et Paris 7, CNRS-IN2P3, Paris, France*
[ac] *Laboratoire de Physique Subatomique et de Cosmologie (LPSC), Université Joseph Fourier, INPG, CNRS-IN2P3, Grenoble, France*
[ad] *SUBATECH, CNRS-IN2P3, Nantes, France*
[ae] *Bergische Universität Wuppertal, Wuppertal, Germany*
[af] *Karlsruhe Institute of Technology – Campus North – Institut für Kernphysik, Karlsruhe, Germany*
[ag] *Karlsruhe Institute of Technology – Campus North – Institut für Prozessdatenverarbeitung und Elektronik, Karlsruhe, Germany*
[ah] *Karlsruhe Institute of Technology – Campus South – Institut für Experimentelle Kernphysik (IEKP), Karlsruhe, Germany*
[ai] *Max-Planck-Institut für Radioastronomie, Bonn, Germany*

[aj] RWTH Aachen University, III. Physikalisches Institut A, Aachen, Germany
[ak] Universität Hamburg, Hamburg, Germany
[al] Universität Siegen, Siegen, Germany
[am] Dipartimento di Fisica dell'Università and INFN, Genova, Italy
[an] Università dell'Aquila and INFN, L'Aquila, Italy
[ao] Università di Milano and Sezione INFN, Milan, Italy
[ap] Dipartimento di Fisica dell'Università del Salento and Sezione INFN, Lecce, Italy
[aq] Università di Napoli "Federico II" and Sezione INFN, Napoli, Italy
[ar] Università di Roma II "Tor Vergata" and Sezione INFN, Roma, Italy
[as] Università di Catania and Sezione INFN, Catania, Italy
[at] Università di Torino and Sezione INFN, Torino, Italy
[au] Dipartimento di Ingegneria dell'Innovazione dell'Università del Salento and Sezione INFN, Lecce, Italy
[av] Istituto di Astrofisica Spaziale e Fisica Cosmica di Palermo (INAF), Palermo, Italy
[aw] Istituto di Fisica dello Spazio Interplanetario (INAF), Università di Torino and Sezione INFN, Torino, Italy
[ax] INFN, Laboratori Nazionali del Gran Sasso, Assergi (L'Aquila), Italy
[ay] Università di Palermo and Sezione INFN, Catania, Italy
[az] Benemérita Universidad Autónoma de Puebla, Puebla, Mexico
[ba] Centro de Investigación y de Estudios Avanzados del IPN (CINVESTAV), México, D.F., Mexico
[bb] Universidad Michoacana de San Nicolas de Hidalgo, Morelia, Michoacan, Mexico
[bc] Universidad Nacional Autonoma de Mexico, Mexico, D.F., Mexico
[bd] IMAPP, Radboud University, Nijmegen, Netherlands
[be] Kernfysisch Versneller Instituut, University of Groningen, Groningen, Netherlands
[bf] NIKHEF, Amsterdam, Netherlands
[bg] ASTRON, Dwingeloo, Netherlands
[bh] Institute of Nuclear Physics PAN, Krakow, Poland
[bi] University of Łódź, Łódź, Poland
[bj] LIP and Instituto Superior Técnico, Lisboa, Portugal
[bk] J. Stefan Institute, Ljubljana, Slovenia
[bl] Laboratory for Astroparticle Physics, University of Nova Gorica, Slovenia
[bm] Instituto de Física Corpuscular, CSIC-Universitat de València, Valencia, Spain
[bn] Universidad Complutense de Madrid, Madrid, Spain
[bo] Universidad de Alcalá, Alcalá de Henares (Madrid), Spain
[bp] Universidad de Granada & C.A.F.P.E., Granada, Spain
[bq] Universidad de Santiago de Compostela, Spain
[br] Rudolf Peierls Centre for Theoretical Physics, University of Oxford, Oxford, United Kingdom
[bs] School of Physics and Astronomy, University of Leeds, United Kingdom
[bt] Argonne National Laboratory, Argonne, IL, USA
[bu] Case Western Reserve University, Cleveland, OH, USA
[bv] Colorado School of Mines, Golden, CO, USA
[bw] Colorado State University, Fort Collins, CO, USA
[bx] Colorado State University, Pueblo, CO, USA
[by] Fermilab, Batavia, IL, USA
[bz] Louisiana State University, Baton Rouge, LA, USA
[ca] Michigan Technological University, Houghton, MI, USA
[cb] New York University, New York, NY, USA
[cc] Northeastern University, Boston, MA, USA
[cd] Ohio State University, Columbus, OH, USA
[ce] Pennsylvania State University, University Park, PA, USA
[cf] Southern University, Baton Rouge, LA, USA
[cg] University of California, Los Angeles, CA, USA
[ch] University of Chicago, Enrico Fermi Institute, Chicago, IL, USA
[ci] University of Nebraska, Lincoln, NE, USA
[cj] University of New Mexico, Albuquerque, NM, USA
[ck] University of Wisconsin, Madison, WI, USA
[cl] University of Wisconsin, Milwaukee, WI, USA
[cm] Institute for Nuclear Science and Technology (INST), Hanoi, Viet Nam

ARTICLE INFO

Article history:
Received 26 June 2010
Received in revised form 26 August 2010
Accepted 31 August 2010
Available online 7 September 2010

Keywords:
Cosmic rays
UHECR

ABSTRACT

Data collected by the Pierre Auger Observatory through 31 August 2007 showed evidence for anisotropy in the arrival directions of cosmic rays above the Greisen–Zatsepin–Kuz'min energy threshold, 6×10^{19} eV. The anisotropy was measured by the fraction of arrival directions that are less than 3.1° from the position of an active galactic nucleus within 75 Mpc (using the Véron-Cetty and Véron 12th catalog). An updated measurement of this fraction is reported here using the arrival directions of cosmic rays recorded above the same energy threshold through 31 December 2009. The number of arrival directions has increased from 27 to 69, allowing a more precise measurement. The correlating fraction is $\left(38^{+7}_{-6}\right)\%$, compared with 21% expected for isotropic cosmic rays. This is down from the early estimate of $\left(69^{+11}_{-13}\right)\%$.

[1] Deceased.
[2] At: Caltech, Pasadena, USA.
[3] At: Konan University, Kobe, Japan.

Anisotropy
Pierre Auger Observatory
Extra-galactic
GZK

The enlarged set of arrival directions is examined also in relation to other populations of nearby extragalactic objects: galaxies in the 2 Microns All Sky Survey and active galactic nuclei detected in hard X-rays by the Swift Burst Alert Telescope. A celestial region around the position of the radiogalaxy Cen A has the largest excess of arrival directions relative to isotropic expectations. The 2-point autocorrelation function is shown for the enlarged set of arrival directions and compared to the isotropic expectation.

1. Introduction

The astrophysical sites of origin of ultra high-energy cosmic rays (UHECRs) remain elusive after almost a half century since a cosmic ray (CR) with energy around 10^{20} eV was first reported [1]. Anisotropy in the arrival directions of UHECRs is expected to provide significant clues for identifying their sources. Protons and nuclei with these energies interact with the cosmic microwave background (CMB), either by pion photoproduction or by nuclear photodisintegration. This interaction limits the distance from which a source can contribute significantly to the flux on Earth, as predicted by Greisen [2] and by Zatsepin and Kuz'min [3] (the GZK effect). For instance, most of the observed flux above 60 EeV (1 EeV $\equiv 10^{18}$ eV) should come from sources within a "GZK horizon" which is approximately 200 Mpc. Processes that could accelerate particles up to such energies require special astrophysical conditions [4]. Few classes of astrophysical objects, such as active galactic nuclei, radiogalaxy lobes and sources of gamma-ray bursts, meet these requirements. Inhomogeneities in their spatial distribution within the GZK horizon may imprint a detectable anisotropy in the UHECR arrival directions. Comparing the arrival directions with the celestial positions of different types of astronomical objects is a useful tool for identifying the sources provided intervening magnetic fields do not deflect the cosmic ray trajectories through large angles.

The flux of UHECRs is extraordinarily small, approximately one particle per square kilometre per century above 60 EeV. Large detection areas are essential. This is achieved by measuring the cosmic rays indirectly through the extensive air showers (EAS) that they produce in the atmosphere. Two complementary techniques are currently used: the measurement of the fluorescence light induced in the atmosphere by the particles in the EAS and the detection of the secondary particles at ground level using an array of surface detectors. The Pierre Auger Observatory implements air fluorescence and water-Cherenkov detection in a hybrid instrument with an aperture of 7000 km^2 sr. The implementation of the baseline design for the Southern Auger Observatory in Argentina [5] was completed in June 2008.

Using data collected through 31 August 2007, the Pierre Auger Collaboration reported in [6,7] a correlation between the arrival directions of UHECRs with energies exceeding 56 EeV and the positions of nearby objects from the 12th edition of the catalog of quasars and active galactic nuclei (AGNs) by Véron-Cetty and Véron [8] (VCV catalog). The null hypothesis of isotropy was rejected with 99% confidence based on a single-trial test that was motivated by early data and confirmed by data collected subsequent to the definition of the test. This correlation with nearby extragalactic objects is consistent with cosmic rays from more distant sources having lost energy in accordance with the flux suppression seen in the measured energy spectrum [9–11] and the GZK expectation. However, the VCV correlation is not sufficient to identify individual sources or a specific class of astrophysical sites of origin. The VCV catalog is a compilation of known AGNs that is neither homogeneous nor statistically complete. Moreover, active galaxies in this catalog trace the nearby large-scale matter distribution, and that includes all types of candidate astrophysical sources, not only AGNs and their subclasses. Analyses comparing the Auger data reported in [6,7] with different types of nearby extragalactic objects can be found in [12–22].

This paper reports the arrival directions of CRs measured with the Pierre Auger Observatory up to 31 December 2009 that have energies above the same threshold as those reported in [6,7]. The data set has increased from 27 to 69 CR events, and is described in Section 2.

In Section 3 we update the measured fraction of CR arrival directions which correlate with the positions of objects in the VCV catalog. The measurement uses identical parameters as in the test reported in [6,7].

In Section 4 we examine the 69 arrival directions with regard to their correlation with populations of nearby extragalactic objects characterised by alternative catalogs. We compare the pattern of the arrival directions with that of the overall matter distribution in the local universe as traced by the galaxies in the 2MASS Redshift Survey (2MRS) [23,24], which is the most densely sampled all-sky redshift survey to date, and with AGNs detected in X-rays with the Swift Burst Alert Telescope (BAT) [25,26].

In Section 5 the intrinsic clustering properties of arrival directions are characterised using their autocorrelation function. We also analyse the region with the largest excess of arrival directions compared to isotropic expectations.

Section 6 summarises the results and potential implications. Some details relating to the 69 UHECRs above 55 EeV are tabulated in the appendix.[4]

2. The Observatory and the dataset

The Pierre Auger Southern Observatory is located in the Province of Mendoza, Argentina (35.1°–35.5°S, 69.0°–69.6°W, 1400 m a.s.l.). The surface array consists of 1600 water-Cherenkov detectors laid out over 3000 km^2 on a triangular grid of 1.5 km spacing. It has been in operation since 1 January 2004, increasing its size from 154 detectors up to 1600 by June 2008. Features of the Observatory that are relevant to the present analysis, that include data taken between 1 January 2004 and 31 December 2009, are outlined below.

The trigger requirement for the surface detector is based on a 3-fold coincidence, satisfied when a triangle of neighboring stations is triggered. A fiducial cut is applied to triggered events to ensure adequate containment inside the array. The cut requires that at least five active stations surround the station with the highest signal, and that the reconstructed shower core be inside a triangle of active detectors. For CR primary energies above 3×10^{18} eV, the efficiency of this trigger chain is 100% [27]. The exposure is determined by purely geometrical considerations, the uncertainty being less than 3%. Note that analyses involving a flux calculation, such as the measurement of the cosmic ray spectrum [9,10], use stricter fiducial cuts, which amount to a lower exposure.

The arrival directions are obtained through the differences in the time of flight of the shower front among the triggered detectors. The angular resolution is defined as the angular radius around

[4] The list of the first 27 events was published in [7]. Since then, the reconstruction algorithms and calibration procedures of the Pierre Auger Observatory have been updated and refined. The lowest energy among the same 27 events (which was 57 EeV in [7]) is 55 EeV according to the latest reconstruction.

Table 1
Summary of correlations within 3.1° between CRs with $E \geqslant 55$ EeV and AGNs in the VCV catalog with redshift $z \leqslant 0.018$. N is the number of CRs measured. k is the number of correlating arrival directions. k_{iso} is the number of correlations expected by chance if the flux were isotropic. P is the cumulative binomial probability to detect k or more correlations from an isotropic distribution. Probabilities are not shown for data sets which include period I because parameters were selected to optimise the correlation in that period.

Period	Dates	Exposure (km^2 sr y)	N	k	k_{iso}	P
I	1 January 2004–26 May 2006	4390	14	8	2.9	–
II	27 May 2006–31 August 2007	4500	13	9	2.7	2×10^{-4}
III	1 September 2007–31 December 2009	11,480	42	12	8.8	0.15
Total	1 January 2004–31 December 2009	20,370	69	29	14.5	–
II + III	27 May 2006–31 December 2009	15,980	55	21	11.6	$\mathbf{3 \times 10^{-3}}$

the true cosmic ray direction that would contain 68% of the reconstructed shower directions. It is cross-checked using events detected simultaneously with the fluorescence detector, *i.e.* hybrid events. It is better than 0.9° for events that trigger at least six surface stations ($E \gtrsim 10$ EeV) [28]. We have tested that the angular resolution has been stable within 0.1° during the period of the present analysis.

The estimator for the primary energy is the reconstructed signal at 1000 m from the shower core, denoted $S(1000)$. The conversion from this estimator to energy is derived experimentally through the use of a subset of showers detected simultaneously with the fluorescence detector and the surface array. The energy resolution is about 15% and the absolute energy scale has a systematic uncertainty of 22% [9,10]. We have checked the time-stability of the energy assignment by computing the fluxes in the energy range from 10 to 55 EeV for five different periods with similar exposure. The fluxes obtained for period I and period II and for three equi-exposure intervals in period III (see Table 1 for the definition of periods I, II and III) are 0.208, 0.222, 0.234, 0.223 and 0.226 km^{-2} sr^{-1} y^{-1}, respectively, each with an uncertainty of 0.008 km^{-2} sr^{-1} y^{-1}, corresponding to ~1000 events in each interval. Given the spectral slope of 2.6 in this energy range [10] and with the assumption of constant flux, this implies that the energy resolution of the Observatory has been stable to 5% over the six years of data taking. The fluxes derived from the small number of events above 55 EeV are similarly constant.

In the present analysis, we consider events recorded with the surface detector between 1 January 2004 and 31 December 2009 with zenith angles $\theta \leqslant 60°$ and reconstructed energy $E \geqslant 55$ EeV: 69 events satisfy these cuts. The integrated exposure for this event selection is 20,370 km^2 sr y. The exposure and statistics of events in different data-taking periods are given in Table 1. The arrival directions and energies are listed in the appendix.

3. Update of the correlation study with AGNs in the VCV catalog

The data reported in [6,7] (periods I and II in Table 1) consist of 27 CR events with energy larger than $E_{th} = 55$ EeV (in the present energy calibration). These data provided evidence for anisotropy in the arrival directions of cosmic rays with the highest energies.

The confidence level for the rejection of the isotropic hypothesis was established through a specific test using prescribed parameters. Using data of period I, the values of the energy threshold, maximum angular separation, and maximum redshift were chosen as those that minimised the probability that the correlation with AGNs in the VCV catalog could occur by chance if the flux were isotropic. The test was then performed using data collected subsequent to the parameter specification by the exploratory scan. It measured the fraction of arrival directions that are less than 3.1° from the position of an AGN within 75 Mpc in the VCV catalog. The fraction expected under the isotropic hypothesis is 21%. The correlation was measured with exactly the same reconstruction algorithms, energy calibration and quality cuts for event selection as in the exploratory scan. With 6 out of 8 events correlated, the test established a 99% confidence level for rejecting the hypothesis that the distribution of arrival directions is isotropic.

The number of correlations within 3.1° between the 69 arrival directions of CRs with $E \geqslant 55$ EeV detected up to 31 December 2009 and AGNs in the VCV catalog with redshift $z \leqslant 0.018$ are summarised in Table 1 and illustrated in Fig. 1.[5] The CR events additional to those reported in [6,7] are the 42 listed for period III. Of those 42 new arrival directions, 12 of them correlate with objects in the VCV catalog defined by the prescribed parameters. The number of correlations expected by chance if the arrival directions were isotropically distributed is 8.8.

The updated estimate of the degree of correlation must include periods II and III only, because the parameters were chosen to maximize the correlation in period I. In Fig. 2 we plot the degree of correlation (p_{data}) with objects in the VCV catalog as a function of the total number of time-ordered events observed during periods II and III. For each additional event the most likely value of p_{data} is k/N (number correlating divided by the cumulative number of arrival directions).

The confidence level intervals in the plot contain 68.3%, 95.45% and 99.7% of the posterior probability for p_{data} given the measured values of k and N. The posterior probability distribution is $p_{data}^k(1-p_{data})^{N-k}(N+1)!/k!(N-k)!$, corresponding to a binomial likelihood with a flat prior. The upper and lower limits in the confidence intervals are chosen such that the posterior probability of every point inside the interval is higher than that of any point outside. The amount of correlation observed has decreased from $(69^{+11}_{-13})\%$, with 9 out of 13 correlations measured in period II, to its current estimate of $(38^{+7}_{-6})\%$, based on 21 correlations out of a total of 55 events in periods II and III.

The cumulative binomial probability that an isotropic flux would yield 21 or more correlations is $P = 0.003$. This updated measurement with 55 events after the initial scan is *a posteriori*, with no prescribed rule for rejecting the hypothesis of isotropy as in [6,7]. No unambiguous confidence level for anisotropy can be derived from the probability $P = 0.003$. P is the probability of finding such a correlation assuming isotropy. It is not the probability of isotropy given such a correlation.

We note that 9 of the 55 events detected in periods II and III are within 10° of the galactic plane, and none of them correlates within 3.1° with the astronomical objects under consideration. Incompleteness of the VCV catalog due to obscuration by the Milky Way or larger magnetic bending of CR trajectories along the galactic disk are potential causes for smaller correlation of arrival directions at small galactic latitudes. If the region within 10° of the galactic plane is excluded the correlation is $(46 \pm 6)\%$ (21 correlations out of 46 events), while 24% is the chance expectation for an isotropic flux.[6]

[5] Differences with the numbers reported in [6,7,29] arise from small differences in the reconstruction of the arrival directions, as detailed in the appendix.

[6] The choice of the size of the region excluded has some arbitrariness. We used 12° in [6,7]. We use 10° here for uniformity with the analysis of the 2MRS catalog in Section 4.

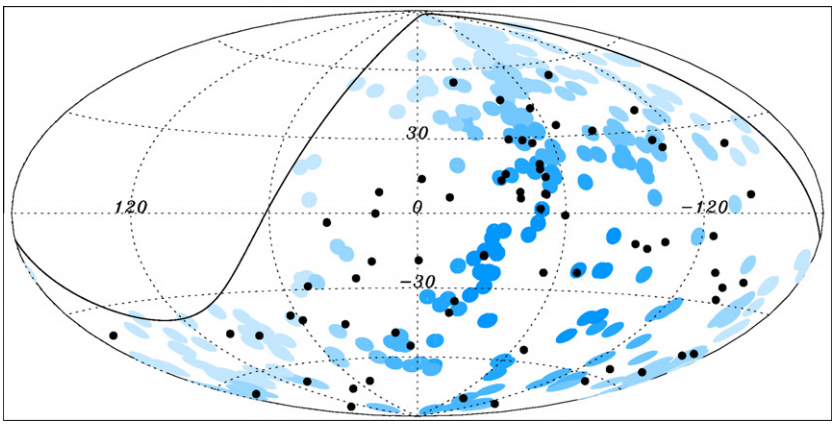

Fig. 1. The 69 arrival directions of CRs with energy $E \geqslant 55$ EeV detected by the Pierre Auger Observatory up to 31 December 2009 are plotted as black dots in an Aitoff-Hammer projection of the sky in galactic coordinates. The solid line represents the border of the field of view of the Southern Observatory for zenith angles smaller than 60°. Blue circles of radius 3.1° are centred at the positions of the 318 AGNs in the VCV catalog that lie within 75 Mpc and that are within the field of view of the Observatory. Darker blue indicates larger relative exposure. The exposure-weighted fraction of the sky covered by the blue circles is 21%. (For interpretation of the references to colour in this figure legend, the reader is referred to the web version of this article.)

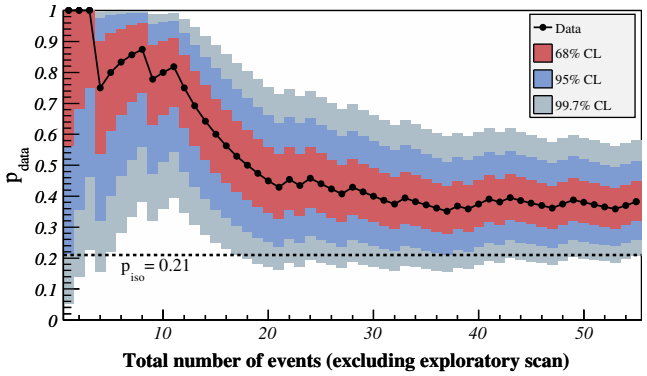

Fig. 2. The most likely value of the degree of correlation $p_{\rm data} = k/N$ is plotted with black dots as a function of the total number of time-ordered events (excluding those in period I). The 68%, 95% and 99.7% confidence level intervals around the most likely value are shaded. The horizontal dashed line shows the isotropic value $p_{\rm iso} = 0.21$. The current estimate of the signal is $\left(0.38^{+0.07}_{-0.06}\right)$.

It has not escaped our notice that the directions of the five most energetic events are not part of the fraction of events that correlate with objects in the VCV catalog.

Additional monitoring of the correlation signal with this set of astronomical objects can also be found in [29]. Further studies of the correlation exploring other parameters are currently in progress. One conjecture often made in the literature (see e.g. [30,31] and references therein) is that powerful radiogalaxies are the most promising contenders for UHECR acceleration, along with gamma-ray bursts. The analysis of directional correlations of UHECRs with positions of AGNs from the VCV catalog discussed here does not account for any differences among those AGNs. Thus, a logical next step with respect to [6,7] would consider the AGN radio luminosity given in the VCV catalog as a fourth scan parameter to find a threshold in radio luminosity above which the directional correlation starts to increase. Such a scan has been performed with a subset of the data and the signal evolution with those parameters is being monitored since, similarly as presented here for all AGN of the VCV. These results will be reported elsewhere.

The HiRes collaboration has reported [32] an absence of a correlation with AGNs of the VCV catalog using the parameters of the Auger prescribed test. They found two events correlating out of a set of 13 arrival directions that have been measured stereoscopically above an energy which they estimated to be the same as the Auger prescribed energy threshold. The 38% correlation measured by Auger suggests that approximately five arrival directions out of 13 HiRes directions should correlate with an AGN position. The difference between 2 and 5 does not rule out a 38% correlation in the northern hemisphere that is observed by the HiRes detector. Also, it is not necessarily expected that the correlating fraction should be the same in both hemispheres. The three-dimensional AGN distribution is not uniform, and the VCV catalog itself has different level of completeness in the two hemispheres. In addition, comparison of results between the two observatories is especially challenging in this situation because the energy cut occurs where the GZK suppression has steepened the already steep cosmic ray spectrum. A small difference in the threshold energy or a difference in energy resolution can strongly affect the measurement of a correlation that exists only above the threshold.

It is worth mentioning that while the degree of correlation with the parameters of the test updated here has decreased with the accumulation of new data, a re-scan of the complete data set similar to that performed in Ref. [7] does not lead to a much more significant correlation for other values of the parameters. The largest departure from isotropic expectations in the scan actually occurs for the same energy threshold $E_{th} = 55$ EeV and maximum redshift $z \leqslant 0.018$. There is a spread in the angular scales over which the correlation departs from isotropic expectations. This issue will be examined in Section 4, where we explore the correlation with other sets of nearby extragalactic objects, described by catalogs more uniform than the VCV compilation.

There is now available a more recent version of the VCV catalog [33]. Conclusions are similar if the arrival directions are compared to the distribution of objects in this latest version.

4. Examination of the arrival directions in relation to other catalogs

As noted in [6], "the correlation that we observe with nearby AGNs from the VCV catalog cannot be used alone as a proof that AGNs are the sources. Other sources, as long as their distribution within the GZK horizon is sufficiently similar to that of the AGNs, could lead to a significant correlation between the arrival directions of cosmic rays and the AGNs positions." It is therefore appropriate to investigate the arrival directions of this data set with respect to other scenarios for cosmic ray sources in the local universe.

It is important to note that all of these studies are made *a posteriori*. None of the results can be used to derive unambiguously a confidence level for anisotropy. The single-trial VCV test that was prescribed in 2006 resulted in 99% confidence that the flux of cosmic rays is not isotropic [6,7]. The *P*-value 0.003 reported in Section 3 does not increase confidence in anisotropy beyond what was reported in [6,7]. With the currently estimated correlation fraction of 38%, a 5σ significance ($P < 6 \times 10^{-7}$) will require 165 events subsequent to period I, and that larger data set will not be available for at least another four years. In the meantime, it is natural to explore the present data set to see if scenarios other than the simple VCV correlation are supported by the current set of arrival directions. Even when (or if) a 5σ deviation from isotropy is established via the VCV correlation, it will be important to determine the best astrophysical interpretation for it. At that time, it could be interesting to test if any of the scenarios investigated here may have acquired additional supporting evidence.

The same minimum energy of CRs will be used for these exploratory studies as was prescribed in 2006 for the VCV test. The idea is to examine the same set of 69 arrival directions using alternative models. Each model has its own set of relevant parameters, and those will be separately tuned. In the prescribed VCV test there were three important parameters. One was the minimum energy that defines the set of arrival directions. The other two were the correlation angle ($\psi = 3.1^\circ$) and the maximum AGN redshift ($z_{max} = 0.018$) which pertain to the model. It would be possible to optimise the minimum energy cut also for every scenario, as was done prior to prescribing the VCV test. For the studies here, however, the data set will be kept the same. It includes all recorded events above 55 EeV. By including period I, which was used to optimise the energy cut for the VCV correlation in that period, scenarios similar to the prescribed VCV model could be favored. The effect of excluding the events used in the exploratory scan, that are strongly correlated with VCV objects, will be analysed.

In what follows we examine the present data set of arrival directions with regard to their correlation with different populations of nearby extragalactic objects: galaxies in the 2MRS catalog and AGNs detected by Swift-BAT. We choose these sets of objects as examples of astrophysical scenarios worthy of examination. We have reported additional explorations (such as the correlation with galaxies in the HI Parkes All Sky Survey [34,35]) in [36].

The 2MRS catalog is the most densely sampled all-sky redshift survey to date. It is a compilation provided by Huchra et al. [23] of the redshifts of the $K_{\rm mag} < 11.25$ brightest galaxies from the 2MASS catalog [24]. It contains approximately 13,000 galaxies within 100 Mpc, and 22,000 within 200 Mpc. It provides an unbiased measure of the distribution of galaxies in the local universe, out to a mean redshift of $z = 0.02$, and to within 10° of the Galactic plane. To avoid biases due to its incompleteness in the galactic plane region, we exclude from all analyses involving this catalog galaxies (as well as CR arrival directions) with galactic latitudes $|b| < 10^\circ$.

The Swift-BAT hard X-ray catalog [25] is the product of the most sensitive all-sky survey in the hard X-ray band. We use the 58-month version of the Swift-BAT survey [26]. A sample of AGNs selected from the hard X-ray band reduces the bias due to absorption that affects an optical selection. We consider for the present analysis all Seyfert galaxies, beamed AGNs, and galaxies likely to be AGN but with no confirmed nuclear activity in the optical spectrum. There are 189 of them within approximately 100 Mpc, and 373 within approximately 200 Mpc.

4.1. Cross-correlation of cosmic rays and nearby extragalactic objects

We report the result of a direct cross-correlation analysis between arrival directions of CRs and positions of the objects in the 2MRS and Swift-BAT catalogs that lie within 200 Mpc. Each CR arrival direction forms a pair with every object in the catalogs. For the cross-correlation estimator, we use the fractional excess (relative to the isotropic expectation) of pairs having angular separations smaller than any angle ψ. This is given by $n_p(\psi)/n_p^{\rm iso}(\psi) - 1$, where $n_p(\psi)$ denotes the number of pairs with separation angle less than ψ. Departures from isotropy are higher if arrival directions correlate with regions with larger density of objects.

We plot in Fig. 3 the relative excess of pairs using data (black dots) in the case of 2MRS galaxies (left) and Swift-BAT AGNs (right). The bands in the plot contain the dispersion in 68%, 95% and 99.7% of simulated sets of the same number of events assuming isotropic cosmic rays. The top panels plot the results using all the arrival directions of CRs with $E \geqslant 55$ EeV collected between 1 January 2004 and 31 December 2009: 69 CR events in the case of correlation with Swift-BAT AGNs, and 57 CR events in the case of correlation with galaxies in the 2MRS catalog (for which galactic latitudes $|b| < 10^\circ$ were excluded). The bottom panels plot the results excluding the arrival directions of CRs collected during period I in Table 1, which were used to optimise the energy cut for the VCV correlation in that period: 55 CRs are used in the case of correlation with Swift-BAT AGNs, and 46 CRs in the case of correlation with galaxies in the 2MRS catalog. Features in the plots are comparable if period I is excluded.

We observe correlation in excess of isotropic expectations in all cases. Note however that the existence of cross-correlation does not imply that the arrival directions are distributed in the sky in the same manner as the objects under consideration.

The catalogs of astronomical objects that were used here are flux-limited sets. A similar analysis confronting the arrival directions with a volume-limited subsample of the 2MRS catalog was reported in Ref. [36].

4.2. Statistical tests on smoothed density maps

4.2.1. Smoothed density maps

We test some specific models for the origin of the highest energy CRs based on the astronomical objects in the catalogs considered in the previous section. We build the probability maps of arrival directions of CRs expected from these objects weighted by their flux at the electromagnetic wavelength relevant in the respective survey and by the attenuation factor expected from the GZK effect. Maps are constructed by the weighted superposition of Gaussian distributions centred at each object position with a fixed angular width σ. For each model, the density map has two free parameters: the smoothing angle σ and an isotropic fraction $f_{\rm iso}$. The smoothing angle serves to account for typical (but unknown) magnetic deflections in the CR trajectories. The addition of an isotropic fraction is a way to account for CR trajectories that have been bent by wide angles due to large charges and/or encounters with strong fields.

A large isotropic fraction could also indicate that the model is not using a set of objects that includes all of the contributing CR sources. The missing flux contributed by the relatively fainter sources below the flux-limit of a survey can be estimated if a model for the luminosity distribution is assumed. For instance, in a flux-weighted model based on objects with a luminosity distribution described by a Schechter function [37] in a survey with characteristic depth of 130 Mpc, account taken of the GZK effect with an energy threshold of 60 EeV, the fraction of missing flux is estimated to be of the order of 35% [15]. The faint sources are not expected to be isotropically distributed, and thus an isotropic fraction may not be an accurate representation for the distribution of that missing flux. An alternative to the addition of an isotropic fraction, when selection effects as a function of distance are known, is to divide the observed density of galaxies at a given distance by the

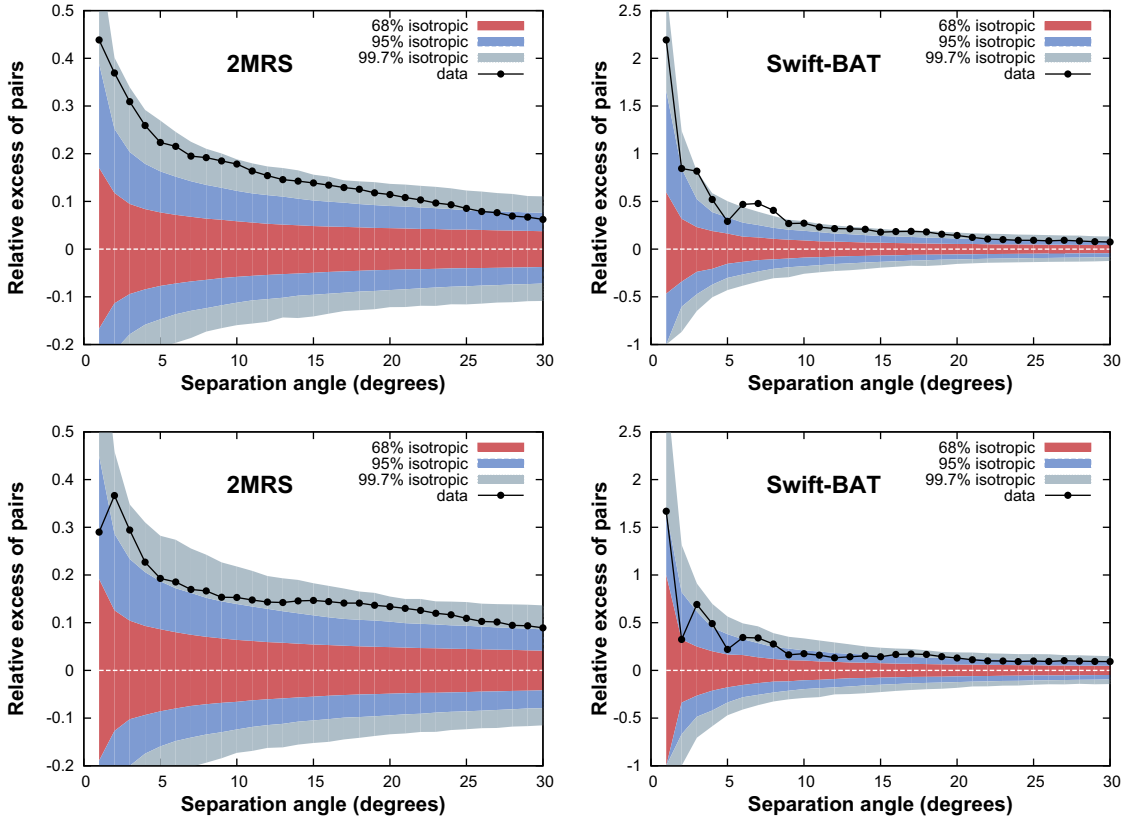

Fig. 3. Cross-correlation between the arrival directions of CRs measured by the Pierre Auger Observatory with $E \geqslant 55$ EeV and positions of 2MRS galaxies (left) and Swift-BAT AGN (right) that lie within 200 Mpc. In the case of 2MRS galactic latitudes (both of galaxies and CRs) are restricted to $|b| > 10^\circ$. The plots in the top panels use all CRs with $E \geqslant 55$ EeV. The plots in the bottom panels exclude data collected during period I in Table 1, that were used to choose the energy threshold and redshift that maximized the correlation with VCV objects in that period. The bands correspond to the 68%, 95% and 99.7% dispersion expected for an isotropic flux.

selection function [38,39]. A possible drawback of this approach is that one assigns the unobserved galaxies to the same locations where bright galaxies are observed, and this may introduce a bias.

We will not assume specific values for the isotropic fraction and smoothing angles introduced into the models, but rather use the data to determine the best-fit values of these parameters.

The smoothed maps are described by a function $F(\hat{\mathbf{n}})$, such that its value in a given direction $\hat{\mathbf{n}}$ is proportional to the probability of detecting a cosmic ray in that direction, according to the model. We write the function $F(\hat{\mathbf{n}})$ as:

$$F(\hat{\mathbf{n}}) = \frac{\varepsilon(\hat{\mathbf{n}})\mu(\hat{\mathbf{n}})}{I}\left[\frac{f_{\rm iso}}{\Omega} + (1 - f_{\rm iso})\frac{\phi(\hat{\mathbf{n}})}{\langle\phi\rangle}\right]. \quad (1)$$

The two terms in the sum between brackets are the isotropic component (parameterised by $f_{\rm iso}$) and the contribution from the astronomical objects. $\Omega = \int \mathrm{d}\Omega\,\mu(\hat{\mathbf{n}})$ is the solid angle subtended by the region of the sky covered by the survey. $\mu(\hat{\mathbf{n}})$ is the mask function of the catalog, that vanishes in the regions of the sky that must be removed (such as that along the galactic plane in the case of the 2MRS catalog) and is unity elsewhere. The flux coming from the objects in the catalog is represented by the term

$$\phi(\hat{\mathbf{n}}) = \sum_{i=1}^{N_{\rm cat}} w(z_i) e^{-\frac{d(\hat{\mathbf{n}}_i,\hat{\mathbf{n}})^2}{2\sigma^2}}, \quad (2)$$

where $d(\hat{\mathbf{n}}_i, \hat{\mathbf{n}})$ is the angle between the direction of the source $\hat{\mathbf{n}}_i$ and the direction of interest $\hat{\mathbf{n}}$. The sum extends over all objects in the catalog, $N_{\rm cat}$. The free parameter σ enables us to take the angular resolution of the Observatory into account and the deflections experienced by cosmic rays under the simplifying method of a gaussian smoothing. A weight $w(z_i)$ is attributed to the ith source located at redshift z_i. We assume a weight proportional to the flux ϕ_i of the source, measured in a given range of wavelengths (X-rays for Swift-BAT and near IR for 2MRS). We multiply it by an attenuation factor due to the GZK suppression, evaluated as the fraction of the events produced above a given energy threshold which are able to reach us from a source at a redshift z with an energy still above that same threshold [15]. We use the GZK suppression factor that corresponds to a proton composition. The suppression is comparable for iron nuclei but is stronger for intermediate mass nuclei. The flux in Eq. (1) is divided by its average $\langle\phi\rangle = \int \mathrm{d}\Omega\mu(\hat{\mathbf{n}})\phi(\hat{\mathbf{n}})$ for normalization. The term in front of the brackets in Eq. (1) is an overall normalization. $\varepsilon(\hat{\mathbf{n}})$ is the relative exposure of the Pierre Auger Observatory, derived analytically from geometric considerations. The constant I is chosen such that the integral of $F(\hat{\mathbf{n}})$ is equal to unity.

We illustrate in Fig. 4 the construction of the smoothed maps with the Swift-BAT catalog of AGNs. The red stars on the left panel of Fig. 4 are centred at the positions of the AGNs, and the area of each star is proportional to the weight of its AGN, determined by the X-ray flux, the relative exposure of the Observatory, and the GZK effect.

The corresponding density map is shown on the right panel of the same figure, smoothed with an angular scale $\sigma = 5^\circ$. No isotropic fraction is built into this map to better illustrate the features of the objects in the catalog. We show the density map obtained for the 2MRS catalog in Fig. 5. Common features can be seen in the two maps.

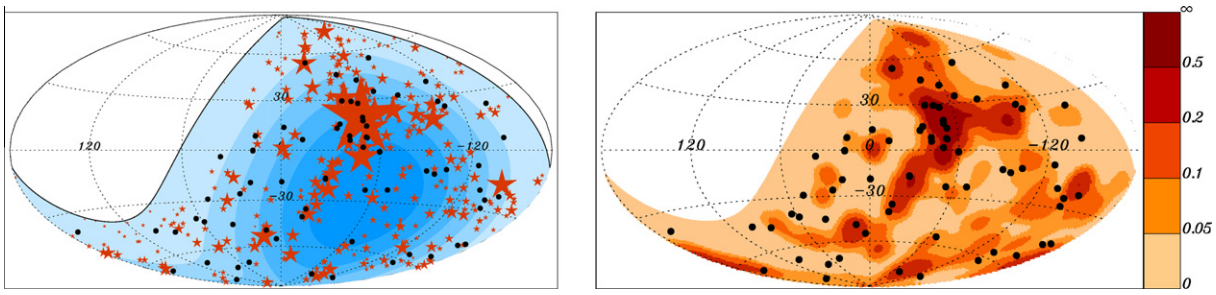

Fig. 4. Left: Sky map in galactic coordinates with the AGNs of the 58-month Swift-BAT catalog plotted as red stars with area proportional to the assigned weight. The solid line represents the border of the field of view of the Southern Observatory. Coloured bands have equal integrated exposure, and darker background colours indicate larger relative exposure. Right: density map derived from the map to the left, smoothed with an angular scale $\sigma = 5^\circ$. The 69 arrival directions of CRs with energy $E \geqslant 55$ EeV detected with the Pierre Auger Observatory are plotted as black dots. (For interpretation of the references to colour in this figure legend, the reader is referred to the web version of this article.)

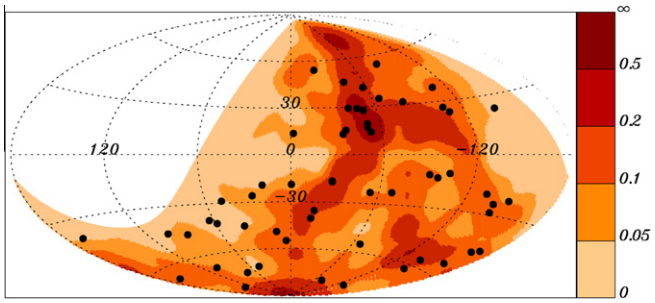

Fig. 5. Cosmic ray density map for the flux-weighted 2MRS galaxies, smoothed with an angular scale $\sigma = 5^\circ$. The black dots are the arrival directions of the CRs with energy $E \geqslant 55$ EeV detected with the Pierre Auger Observatory. Galactic latitudes are restricted to $|b| > 10^\circ$, both for galaxies and CR events.

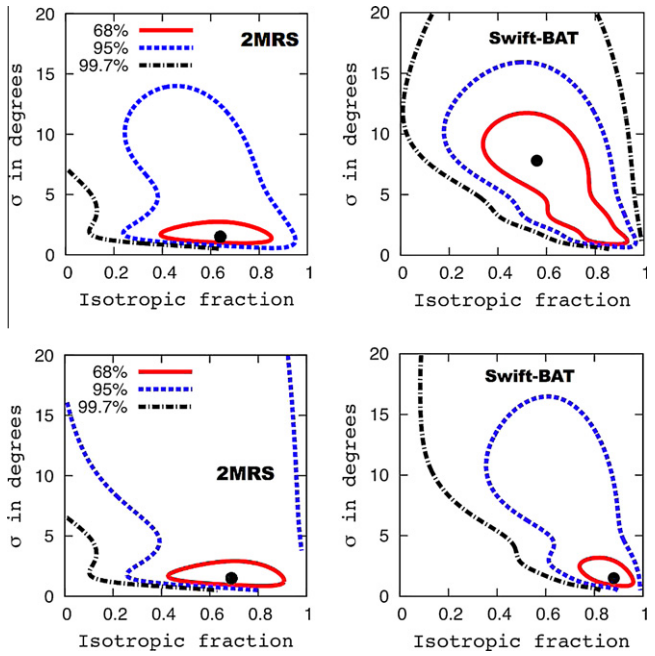

Fig. 6. Confidence intervals for the parameters $(\sigma, f_{\rm iso})$ derived from the likelihood function using the arrival directions of CRs with $E \geqslant 55$ EeV for the two models considered: 2MRS galaxies (left) and Swift-BAT AGNs (right). The pair of parameters that maximize the likelihood is indicated by a black dot. The plots in the top panels use all data. The plots in the bottom panels exclude data collected during period I in Table 1, that were used to choose the energy threshold that maximized the correlation with VCV objects in that period. In the case of 2MRS galactic latitudes (both of galaxies and CRs) are restricted to $|b| > 10^\circ$.

4.2.2. Likelihood test

For each model and for different values of the smoothing angle σ and isotropic fraction $f_{\rm iso}$ we evaluate the log-likelihood of the data sample:

$$\mathcal{LL} = \sum_{k=1}^{N_{\rm data}} \ln F(\hat{\mathbf{n}}_{\mathbf{k}}), \tag{3}$$

where $\hat{\mathbf{n}}_{\mathbf{k}}$ is the direction of the kth event.

We consider the models based on 2MRS and Swift-BAT objects weighted by their flux in the respective wavelength. The top panels in Fig. 6 plot the results using all the arrival directions of CRs with $E \geqslant 55$ EeV. The bottom panels plot the results excluding the CRs collected during period I in Table 1, which were used to optimise the energy cut for the VCV correlation in that period. The best-fit values of $(\sigma, f_{\rm iso})$ are those that maximize the likelihood of the data sample, and are indicated by a black dot. Contours of 68%, 95% and 99.7% confidence intervals are shown. The best-fit values of $(\sigma, f_{\rm iso})$ are (1.5°, 0.64) for 2MRS and (7.8°, 0.56) for Swift-BAT using all data. With data in period I excluded the best-fit parameters are (1.5°, 0.69) for 2MRS and (1.5°, 0.88) for Swift-BAT. These values are not strongly constrained with the present statistics. Notice for instance that the best-fit value of $f_{\rm iso}$ for the Swift-BAT model increases from 0.56 to 0.88 and σ decreases from 7.8° to 1.5° if data in period I is excluded. More data is needed to discern if it is the correlation on small angles of a few events with the very high-density regions of this model (such as the region in the direction to the radiogalaxy Centaurus A, the object with the largest weight in Fig. 4) that masks a potentially larger correlating fraction (hence a smaller $f_{\rm iso}$) over larger angular scales.

Finding the values of σ and $f_{\rm iso}$ that maximize the log-likelihood does not ensure that the model fits well the data. To test the compatibility between data and model, we generate simulated sets with the same number of arrival directions as in the data, drawn either from the density map of the models or isotropically. We then compare the distributions of the mean log-likelihood $(\mathcal{LL}/N_{\rm data})$ with the value obtained for the data. We present the results in Fig. 7.

Data are compatible with the models and differ from average isotropic expectations. The fraction f of isotropic realizations that have a higher likelihood than the data is 2×10^{-4} in the case of the model based on Swift-BAT AGNs, and 4×10^{-3} with the model based on 2MRS galaxies. These values of f are obtained with the parameters σ and $f_{\rm iso}$ that maximize the likelihood for the respective catalog using all the events with energy larger than 55 EeV (the black dots in the top panels of Fig. 6). With the same parameters, and data from period I excluded, $f \approx 0.02$ in both models.

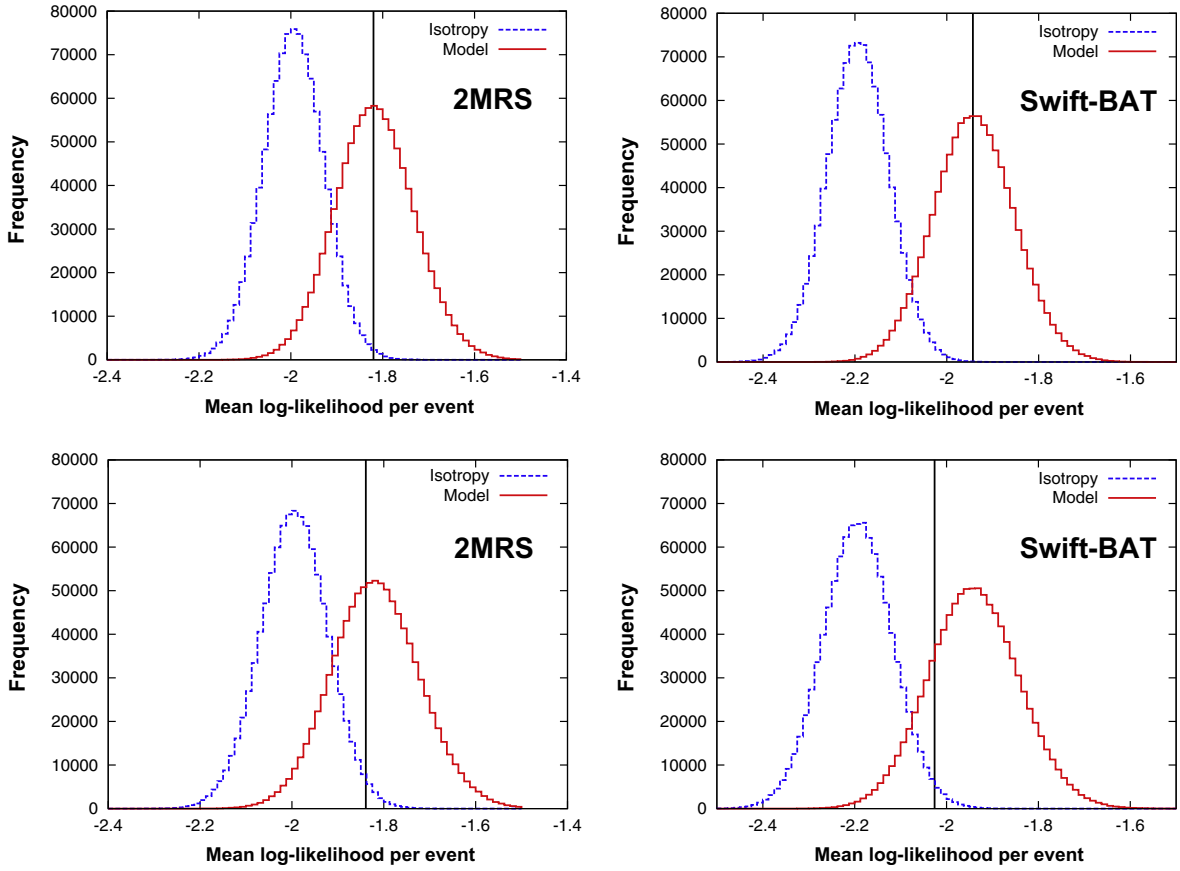

Fig. 7. Distributions of mean log-likelihood per event for isotropic arrival directions (blue, solid line histogram) and for the model predictions (red, dashed line histogram). The parameters for the models based on the 2MRS galaxies (left) and Swift-BAT AGNs (right) are those that maximize the likelihood with all data, namely (1.5°, 0.64) for 2MRS and (7.8°, 0.56) for Swift-BAT. The value of the log-likelihood for the data is indicated by a black vertical line. The plots in the top panels use all data, and those in the bottom panels exclude data collected during period I. (For interpretation of the references to colour in this figure legend, the reader is referred to the web version of this article.)

These figures are *a posteriori*, and do not represent a confidence level on anisotropy.

The likelihood test is sensitive to whether or not the data points lie in a high-density region of the model. Complementary methods can be applied that test the overall proportionality between the sky distribution of arrival directions and model predictions. For instance in Ref. [36] we have developed a method based on the smoothed density maps that simultaneously tests both the correlation as well as the intrinsic clustering properties of the data compared to the models. These tests are inconclusive with present data. The dispersion in the predictions by different models decreases with an increasing number of events. For instance, the width of the histograms in Fig. 7 decreases as $1/\sqrt{N}$. With this dispersion reduced by a factor two, if the anisotropy is substantiated by future data it should also become possible to narrow the range of viable astrophysical scenarios.

The HiRes collaboration has reported [40] that their data with threshold energies of 57 EeV are incompatible at a 95% confidence level with a matter tracer model based on 2MRS galaxies with smoothing angles smaller than 10°. The analysis performed in [40] has the smoothing angle as the only free parameter. As already mentioned at the end of Section 3, comparison of results between the two observatories is especially challenging around the GZK energy threshold. Auger arrival directions are compatible with models of the local matter distribution based on 2MRS galaxies for smoothing angles of a few degrees and correlating fractions of about 40% ($f_{\rm iso} \approx 0.6$ is required for the best fit).

5. Other aspects of the arrival directions

The autocorrelation of the arrival directions can provide information about clustering without reference to any catalog. We show in Fig. 8 the autocorrelation function for the set of the 69 events with $E \geqslant 55$ EeV. The number of pairs of events with an angular separation smaller than a given value are plotted as black dots. The 68%, 95% and 99.7% dispersion expected in the case of an isotropic flux is represented by coloured bands. For angles greater than 45° (not shown) the black dots lie within the 68% band. The region of small angular scale is shown separately for better resolution.

The largest deviation from the isotropic expectation occurs for an angular scale of 11°, where 51 pairs have a smaller separation compared with 34.8 pairs expected. In isotropic realizations of 69 events, a fraction $f(11^\circ) = 0.013$ have 51 or more pairs within 11°. The fraction of isotropic realizations that achieve $f(\psi) \leqslant 0.013$ for any angle ψ is $P = 0.10$.

The region with the largest overdensity of arrival directions among the 69 CRs with $E \geqslant 55$ EeV, as estimated by the excess above isotropic expectations in circular windows, is centred at galactic coordinates $(l, b) = (-46.4^\circ, 17.7^\circ)$. There are 12 arrival directions inside a window with radius 13° centred in that location, where 1.7 is the isotropic expectation. The centre of this region is only 4° away from the location of the radiogalaxy Cen A (−50.5°, 19.4°) and it is not far from the direction of the Centaurus cluster (−57.6°, 21.6°). It was noted in [6,7] that the arrival directions of

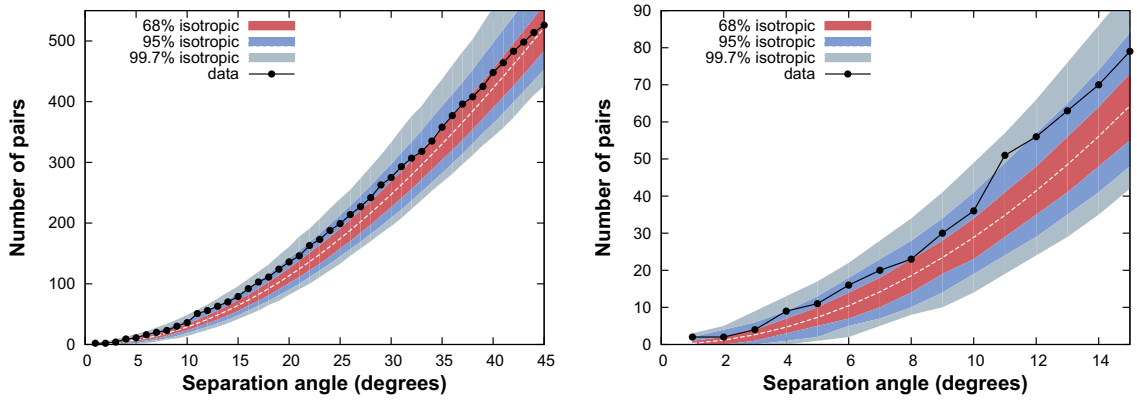

Fig. 8. Cumulative autocorrelation function for the set of 69 events with $E \geqslant 55$ EeV (black dots). The bands correspond to the 68%, 95% and 99.7% dispersion expected for an isotropic flux. The plot in the right panel is an enlarged version of the left plot restricted to angles less than 15°.

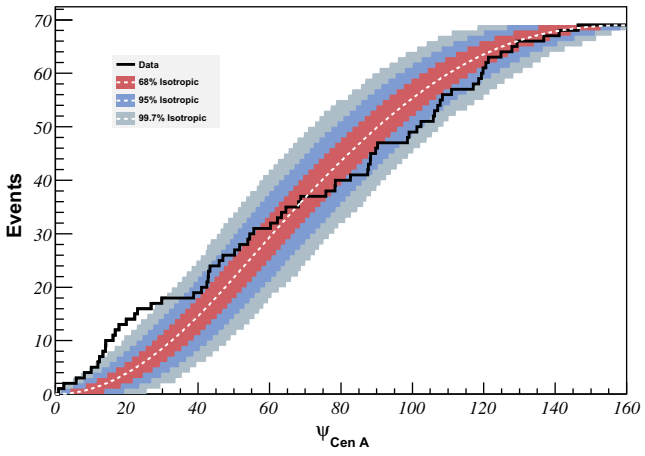

Fig. 9. Cumulative number of events with $E \geqslant 55$ EeV as a function of angular distance from the direction of Cen A. The bands correspond to the 68%, 95% and 99.7% dispersion expected for an isotropic flux.

two CR events correlate with the nucleus position of the radiogalaxy Cen A, while several lie in the vicinity of its radio lobe extension. At only 3.8 Mpc distance, Cen A is the closest AGN. It is obviously an interesting region to monitor with additional data.

We show in Fig. 9 the number of CR arrival directions within a variable angular radius from Cen A. In a Kolmogorov–Smirnov test, 4% of the realizations of 69 arrival directions drawn from an isotropic distribution have a maximum departure from the isotropic expectation greater than or equal to the maximum departure observed in data. The overdensity with largest significance is given by the presence of 13 arrival directions within 18°, in which 3.2 arrival directions are expected if the flux were isotropic.

The CRs in this region of the sky make a dominant contribution to the autocorrelation signal. For instance, the 13 arrival directions that are within 18° from Cen A form six pairs separated by less than 4° and 28 pairs by less than 11°. These events also make a large contribution to the correlation with different populations of nearby extragalactic objects, both because they are in excess above isotropic expectations and because this region is densely populated with galaxies. The flux-weighted models illustrated in Figs. 4 and 5 predict that the fraction of CRs inside a circle with radius 18° centred at the position of Cen A is 13.4% (2MRS) and 29.3% (Swift-BAT), compared to 18.8% observed in data and 4.7% expected if the flux were isotropic.

In contrast to the region around Cen A and the Centaurus cluster, there is a paucity of events from the region around the radiogalaxy M87 and the Virgo cluster. None of the 69 events with $E \geqslant 55$ EeV is within 18° of M87. Due to its northern declination, however, M87 gets only one-third the exposure that Cen A gets at the Southern Auger observatory. Only 1.1 events are expected within that 18° circle for an isotropic flux.

Distance also matters. M87 is five times farther away than Cen A, so the flux would be 25 times less if the sources had equal cosmic ray luminosities. Coupled with the reduced exposure to M87, the recorded arrivals from Cen A would be 75 times those from M87 if the two radiogalaxies were equally luminous in cosmic rays.

The situation is different in comparing the Virgo cluster against the Centaurus cluster. While M87 is near the centre of the Virgo cluster, Cen A is not part of the Centaurus cluster. Both clusters are well within the GZK horizon, but the Centaurus cluster is three times more distant than Virgo. Combining $1/r^2$ flux dependence and the exposure difference, therefore, the recorded events from the Virgo cluster should outnumber those from Centaurus by three-to-one if the two clusters have equal cosmic ray luminosities. The flux-weighted models illustrated in Figs. 4 and 5 predict that the fraction of CRs inside a circle with radius 18° centred at the position of M87 is 6.4% (2MRS) and 3.0% (Swift-BAT), compared to 1.6% expected if the flux were isotropic.

6. Discussion and conclusions

Between January 2004 and December 2009 the Pierre Auger Observatory has detected 69 cosmic rays with energy in excess of 55 EeV. Their arrival directions are reported here. This data set is more than twice as large as the one analysed in [6,7], which provided evidence of anisotropy in CR arrival directions at the 99% confidence level. The anisotropy was tested with *a priori* parameters through the correlation between the arrival directions of CRs and the positions of nearby active galaxies from the VCV catalog. The degree of that observed correlation has decreased from $(69^{+11}_{-13})\%$ to $(38^{+7}_{-6})\%$, to be compared with the 21% expected to occur by chance if the flux were isotropic. More data are needed to determine this correlating fraction accurately.

We have further examined with *a posteriori* explorations the arrival directions of these CRs using different scenarios. We have compared the distribution of arrival directions with the positions of different populations of nearby extragalactic objects: galaxies in the 2MRS survey and AGNs detected in X-rays by Swift-BAT. We have considered models in which the CR luminosity is proportional to the flux in the respective wavelength for the objects in these catalogs. Data are readily compatible with the models for suitable parameters (smoothing angle σ and isotropic fraction $f_{\rm iso}$). The values of these parameters have been obtained for each model

as best fits to the data: they are around a few degrees for σ and between 0.56 and 0.88 for f_{iso}. Large values of f_{iso} may be an indication of catalog incompleteness, or that proportionality between CR luminosity and electromagnetic flux is unrealistic, or that a fraction of the arrival directions are isotropized by large magnetic deflections due to large charges and/or encounters with strong field regions. The best-fit values of σ and f_{iso} are not strongly constrained with the present statistics. These studies are *a posteriori* and do not constitute further quantitative evidence for anisotropy. They show that, at present, there are multiple astrophysical models of anisotropy arising from the distribution of matter in the nearby universe which are fully consistent with the observed distribution of arrival directions.

The autocorrelation of the arrival directions shows only a modest excess of direction pairs over a broad range of small angles. In scenarios of discrete sources in the nearby universe, the absence of strong clustering at small angles can be interpreted as evidence of many contributing sources and/or large angular separations between arrival directions from the same source.

We have analysed the region of the sky close to the location of the radiogalaxy Cen A, since this corresponds to the largest observed excess with respect to isotropic expectations. The CRs in this region make a strong contribution to the autocorrelation signal and to the correlation with different populations of nearby extragalactic objects. From all the arrival directions of CRs with $E \geqslant 55$ EeV, 18.8% lie within 18° of Cen A, while 4.7% is the isotropic expectation. This region is densely populated with different types of nearby extragalactic objects. Flux-weighted models based on 2MRS galaxies and on Swift-BAT AGNs predict a fraction of CRs from this region of 13% and 29% respectively. As reported in 2007 [6,7], there are two arrival directions very close to the position of the Cen A nucleus. Aside from those two events, the excess is distributed rather broadly.

Measurements by the Pierre Auger Observatory [41] of the depth of shower maximum and its fluctuations indicate a trend toward heavy nuclei with increasing energy. Although the measurements available now are only up to about 55 EeV, the trend suggests that primary CRs are likely to be dominated by heavy nuclei at higher energies. This interpretation of the shower depths is not certain, however. It relies on shower simulations that use hadronic interaction models to extrapolate particle interaction properties two orders of magnitude in centre-of-mass energy beyond the regime where they have been tested experimentally. A knowledge of CR composition is important for deciding which of several source scenarios is more likely. The trajectories of highly charged nuclei are expected to undergo large deflections due to the Galaxy's magnetic fields. While a correlation of arrival directions with nearby matter on small angular scales is plausible for protons above 55 EeV, it is puzzling if the CRs are heavy nuclei.

Definitive conclusions must await additional data. The correlation of recent data with objects in the VCV catalog is not as strong as that observed in 2007. If the evidence for anisotropy is substantiated by future data, then it should also become possible to discriminate between different astrophysical scenarios using techniques of the type that have been presented here to explore the compatibility of different models with the present set of arrival directions.

Acknowledgments

The successful installation and commissioning of the Pierre Auger Observatory would not have been possible without the strong commitment and effort from the technical and administrative staff in Malargüe.

We are very grateful to the following agencies and organizations for financial support: Comisión Nacional de Energía Atómica, Fundación Antorchas, Gobierno De La Provincia de Mendoza, Municipalidad de Malargüe, NDM Holdings and Valle Las Leñas, in gratitude for their continuing cooperation over land access, Argentina; the Australian Research Council; Conselho Nacional de Desenvolvimento Científico e Tecnológico (CNPq), Financiadora de Estudos e Projetos (FINEP), Fundação de Amparo à Pesquisa do Estado de Rio de Janeiro (FAPERJ), Fundação de Amparo à Pesquisa do Estado de São Paulo (FAPESP), Ministério de Ciência e Tecnologia (MCT), Brazil; AVCR AV0Z10100502 and AV0Z10100522, GAAV KJB300100801 and KJB100100904, MSMT-CR LA08016, LC527, 1M06002, and MSM0021620859, Czech Republic; Centre de Calcul IN2P3/CNRS, Centre National de la Recherche Scientifique (CNRS), Conseil Régional Ile-de-France, Département Physique Nucléaire et Corpusculaire (PNC-IN2P3/CNRS), Département Sciences de l'Univers (SDU-INSU/CNRS), France; Bundesministerium für Bildung und Forschung (BMBF), Deutsche Forschungsgemeinschaft (DFG), Finanzministerium Baden-Württemberg, Helmholtz-Gemeinschaft Deutscher Forschungszentren (HGF), Ministerium für Wissenschaft und Forschung, Nordrhein-Westfalen, Ministerium für Wissenschaft, Forschung und Kunst, Baden-Württemberg, Germany; Istituto Nazionale di Fisica Nucleare (INFN), Istituto Nazionale di Astrofisica (INAF), Ministero dell'Istruzione, dell'Università e della Ricerca (MIUR), Italy; Consejo Nacional de Ciencia y Tecnología (CONACYT), Mexico; Ministerie van Onderwijs, Cultuur en Wetenschap, Nederlandse Organisatie voor Wetenschappelijk Onderzoek (NWO), Stichting voor Fundamenteel Onderzoek der Materie (FOM), Netherlands; Ministry of Science and Higher Education, Grant Nos. 1 P03 D 014 30 and N N202 207238, Poland; Fundação para a Ciência e a Tecnologia, Portugal; Ministry for Higher Education, Science, and Technology, Slovenian Research Agency, Slovenia; Comunidad de Madrid, Consejería de Educación de la Comunidad de Castilla La Mancha, FEDER funds, Ministerio de Ciencia e Innovación and Consolider-Ingenio 2010 (CPAN), Generalitat Valenciana, Junta de Andalucía, Xunta de Galicia, Spain; Science and Technology Facilities Council, United Kingdom; Department of Energy, Contract Nos. DE-AC02-07CH11359, DE-FR02-04ER41300, National Science Foundation, Grant No. 0450696, The Grainger Foundation USA; ALFA-EC/ HELEN, European Union 6th Framework Program, Grant No. MEIF-CT-2005-025057, European Union 7th Framework Program, Grant No. PIEF-GA-2008-220240, and UNESCO.

Appendix. Event list

We list in the following table the equatorial coordinates (RA, Dec) and the galactic coordinates (l, b) of the 69 events recorded from 1 January 2004 up to 31 December 2009 with $E \geqslant 55$ EeV, together with their date of observation (year and Julian day), zenith angle (θ), signal at 1000 m from the shower core S(1000), and energy E. S(1000) is measured in units called VEM, determined by the average charge deposited by a high-energy down-going vertical and central muon [5]. The energy resolution is about 15% and the absolute energy scale has a systematic uncertainty of 22% [9,10]. The angular resolution is better than 0.9° [28].

In [7] we published the list of the first 27 events, detected in periods I and II in Table 1. Since then, the reconstruction algorithms and calibration procedures of the Pierre Auger Observatory have been updated and refined. The lowest energy among these same 27 events (which was 57 EeV in [7]) is 55 EeV according to the latest reconstruction. The reconstructed values of S(1000) have changed by less than 4% and of the energy by less than 7%. The arrival directions of 26 events differ by less than 0.1° from their previous determination, while 1 differs by 0.4°. The events recorded in the different periods, I, II and III, are separated by horizontal lines.

Year	Julian day	θ (deg)	$S(1000)$ (VEM)	E (EeV)	RA (deg)	Dec (deg)	l (deg)	b (deg)
2004	125	47.7	245	65	267.1	−11.4	15.5	8.4
2004	142	59.3	205	79	199.7	−34.9	−50.7	27.7
2004	282	26.5	329	64	208.1	−60.3	−49.6	1.7
2004	339	44.7	324	83	268.6	−60.9	−27.6	−17.0
2004	343	23.4	321	60	224.5	−44.2	−34.3	13.0
2005	54	35.0	374	81	17.4	−37.9	−75.6	−78.6
2005	63	54.4	214	68	331.2	−1.2	58.7	−42.4
2005	81	17.1	309	55	199.1	−48.5	−52.8	14.1
2005	295	15.4	310	55	332.9	−38.2	4.2	−54.9
2005	306	40.0	248	56	315.4	−0.4	48.8	−28.8
2005	306	14.2	444	80	114.6	−43.0	−103.8	−10.3
2006	35	30.8	396	82	53.7	−7.8	−165.9	−46.9
2006	55	37.9	264	58	267.7	−60.6	−27.5	−16.5
2006	81	34.0	367	78	201.1	−55.3	−52.3	7.3
2006	185	59.0	211	80	350.1	9.5	88.7	−47.2
2006	296	54.0	207	66	53.0	−4.2	−170.7	−45.4
2006	299	26.0	344	66	200.9	−45.3	−51.2	17.2
2007	13	14.3	753	142	192.8	−21.1	−57.2	41.8
2007	51	39.2	255	57	331.7	2.9	63.5	−40.3
2007	69	30.4	334	68	200.2	−43.3	−51.4	19.3
2007	84	17.2	341	61	143.2	−18.3	−109.3	23.8
2007	145	23.9	400	77	47.6	−12.8	−164.0	−54.5
2007	186	44.8	254	64	219.4	−53.8	−41.7	5.8
2007	193	17.9	470	87	325.5	−33.4	12.2	−49.0
2007	221	35.3	318	68	212.7	−3.2	−21.8	54.1
2007	234	33.3	366	77	185.3	−27.9	−65.2	34.5
2007	235	42.6	275	66	105.9	−22.9	−125.2	−7.7
2007	295	21.1	389	73	325.7	−15.6	37.8	−44.8
2007	343	30.9	447	93	81.5	−7.4	−150.1	−22.3
2007	345	51.5	212	62	314.9	−53.4	−15.5	−40.4
2008	13	17.0	363	66	252.8	−22.6	−1.8	13.7
2008	18	50.1	389	115	352.7	−20.9	47.4	−70.5
2008	36	28.4	367	73	186.9	−63.6	−59.7	−0.9
2008	51	20.7	314	58	201.9	−54.9	−51.8	7.6
2008	52	31.7	308	63	82.8	−15.8	−141.2	−24.7
2008	87	39.0	355	82	220.5	−42.9	−36.4	15.5
2008	118	36.2	324	70	110.2	−0.9	−142.9	6.2
2008	192	20.4	302	55	306.7	−55.3	−17.3	−35.4
2008	205	53.0	183	56	358.9	15.5	103.6	−45.3
2008	264	44.4	384	99	116.0	−50.6	−96.4	−12.9
2008	268	49.8	415	123	287.6	1.5	36.4	−3.6
2008	282	28.9	309	61	202.3	−16.1	−44.0	45.8
2008	296	42.8	293	71	15.6	−17.0	137.7	−79.6
2008	322	28.3	345	68	25.1	−61.2	−67.3	−54.9
2008	328	47.2	250	66	126.5	5.3	−140.8	23.4
2008	337	31.0	348	71	275.5	−14.4	16.8	−0.1
2008	362	31.4	406	84	209.6	−31.3	−40.7	29.4
2009	7	59.3	152	57	286.3	−37.6	−0.5	−18.7
2009	30	32.3	346	72	303.9	−16.7	26.6	−25.9
2009	32	56.2	199	67	0.0	−15.4	75.0	−73.3
2009	35	52.8	191	57	227.1	−85.2	−54.1	−23.2
2009	39	42.4	291	70	147.2	−18.3	−106.5	26.6
2009	47	20.8	311	57	78.3	−16.0	−142.9	−28.8
2009	51	7.1	377	65	203.7	−33.1	−46.7	28.9
2009	78	8.2	350	61	26.7	−29.1	−134.6	−77.6
2009	78	27.3	424	84	122.9	−54.6	−90.7	−11.3
2009	80	44.5	263	66	170.1	−27.1	−80.9	31.5
2009	80	18.4	388	71	251.4	−35.8	−13.0	6.3

Event list (*continued*)

Year	Julian day	θ (deg)	$S(1000)$ (VEM)	E (EeV)	RA (deg)	Dec (deg)	l (deg)	b (deg)
2009	160	40.9	242	56	43.8	−25.5	−143.2	−62.3
2009	168	27.0	294	57	153.6	−8.6	−109.4	37.9
2009	191	26.9	339	66	294.5	−20.5	19.1	−19.2
2009	212	52.7	188	57	122.6	−78.5	−68.8	−22.8
2009	219	40.2	252	57	29.4	−8.6	166.1	−65.8
2009	225	26.2	298	57	90.5	−21.3	−132.8	−20.0
2009	262	22.4	341	64	50.1	−25.9	−140.5	−56.7
2009	282	47.2	231	61	47.7	11.5	168.7	−38.6
2009	288	34.2	310	66	217.9	−51.5	−41.6	8.3
2009	304	30.1	304	61	177.7	−5.0	−83.8	54.7
2009	326	31.4	283	57	5.4	−5.6	103.3	−67.3

References

[1] J. Linsley, Phys. Rev. Lett. 10 (1963) 146.
[2] K. Greisen, Phys. Rev. Lett. 16 (1966) 748.
[3] G.T. Zatsepin, V.A. Kuz'min, Sov. Phys. JETP Lett. 4 (1966) 78.
[4] A.M. Hillas, Ann. Rev. Astron. Astrophys. 22 (1984) 425.
[5] The Pierre Auger Collaboration, Nucl. Instrum. Meth. A 523 (2004) 50.
[6] The Pierre Auger Collaboration, Science 318 (2007) 938.
[7] The Pierre Auger Collaboration, Astropart. Phys. 29 (2008) 188.
[8] M.-P. Véron-Cetty, P. Véron, Astron. Astrophys. 455 (2006) 773.
[9] The Pierre Auger Collaboration, Phys. Rev. Lett. 101 (2008) 061101.
[10] The HiRes Collaboration, Phys. Lett. B 685 (2010) 239.
[11] The Pierre Auger Collaboration, Phys. Rev. Lett. 100 (2008) 101101.
[12] T. Kashti, E. Waxman, JCAP 0805 (2008) 006.
[13] M. George, A.C. Fabian, W.H. Baumgartner, R.F. Mushotzky, J. Tueller, Mon. Notice Royal Astron. Soc. 388 (2008) L59.
[14] G. Ghisellini, G. Ghirlanda, F. Tavecchio, F. Fraternali, G. Pareschi, Mon. Notice Royal Astron. Soc. 390 (2008) L88.
[15] D. Harari, S. Mollerach, E. Roulet, Mon. Notice Royal Astron. Soc. 394 (2009) 916.
[16] N.M. Nagar, J. Matulich, Astron. Astrophys. 488 (2008) 879.
[17] A.M. Hillas, Astropart. Phys. 32 (2009) 160.
[18] I.V. Moskalenko, L. Stawarz, T.A. Porter, C.C. Cheung, Astrophys. J. 693 (2009) 1261.
[19] G.R. Farrar, A.A. Berlind, I. Zaw, Astrophys. J. 716 (2010) 914.
[20] T. Wibig, A.W. Wolfendale, Open Astron. J. 2 (2009) 95.
[21] H. Takami, T. Nishimichi, K. Yahata, K. Sato, JCAP 0906 (2009) 031.
[22] H.B.J. Koers, P. Tinyakov, JCAP 0904 (2009) 003.
[23] J. Huchra et al., in: IAU Symposium No. 216, 2005, p. 170; J. Huchra, L. Macri, K. Masters, A. Crook, et al., in preparation.
[24] T.H. Jarrett, T. Chester, R. Cutri, S. Schneider, M. Skrutskie, J.P. Huchra, Astron. J. 119 (2000) 2498.
[25] J. Tueller et al., Astrophys. J. Suppl. 186 (2010) 378.
[26] W. Baumgartner et al., in preparation.
[27] The Pierre Auger Collaboration, Nucl. Instrum. Meth. A 613 (2010) 29.
[28] C. Bonifazi, for The Pierre Auger Collaboration, Nucl. Phys. B (Proc. Suppl.) 190 (2009) 20.
[29] J.D. Hague, for The Pierre Auger Collaboration, Correlation of the highest energy cosmic rays with nearby extragalactic objects in Pierre Auger Observatory Data, in: Presented at the 31st International Cosmic Ray Conference, Łódź, Poland, 2009. arXiv:0906.2347 [astro-ph].
[30] V.L. Ginzburg, S.I. Syrovatskii, The Origin of Cosmic Rays, Pergamon Press, Oxford, 1964 (Original Russian Edition (1963)).
[31] P. Biermann et al., Nucl. Phys. B (Proc. Suppl.) 190 (2009) 61.
[32] The HiRes Collaboration, Astropart. Phys. 30 (2008) 175.
[33] M.-P. Véron-Cetty, P. Véron, Astron. Astrophys. 518 (2010) A10.
[34] M.J. Meyer et al., Mon. Notice Royal Astron. Soc. 350 (2004) 1195.
[35] O.I. Wong et al., Mon. Notice Royal Astron. Soc. 371 (2006) 1855.
[36] J. Aublin, for The Pierre Auger Collaboration, Discriminating potential astrophysical sources of the highest energy cosmic rays with the Pierre Auger Observatory, in: Presented at the 31st International Cosmic Ray Conference, Łódź, Poland, 2009, arXiv:0906.2347 [astro-ph].
[37] P. Schechter, Astrophys. J. 203 (1976) 297.
[38] E. Waxman, K.B. Fisher, T. Piran, Astrophys. J. 483 (1997) 1.
[39] A. Cuoco, R. D' Abrusco, G. Longo, G. Miele, P.D. Serpico, JCAP 0601 (2006) 009.
[40] The HiRes Collaboration, Astrophys. J. 713 (2010) L64.
[41] The Pierre Auger Collaboration, Phys. Rev. Lett. 104 (2010) 091101.